Journal of Solid State Chemistry **168,** 229–236 (2002)
doi:10.1006/jssc.2002.9715

Synthesis and Evolution of the Crystalline Phases in $Ca_{1-x}Sr_xAl_2O_4$

A. K. Prodjosantoso*,† and B. J. Kennedy*,[1]

*The Centre for Heavy Metals Research, School of Chemistry, The University of Sydney, Sydney, NSW 2006, Australia; and †Jurusan Kimia, Universitas Negeri Yogyakarta, Yogyakarta, DIY 55281 Indonesia

Received April 8, 2002; in revised form June 3, 2002; accepted July 16, 2002

The preparation and structural properties of the series of oxides $Ca_{1-x}Sr_xAlO_4$ are described. Using a combination of synchrotron and neutron powder diffraction methods, it is found that the single-phase solid solutions exist only over a very limited range, $x < 0.35$ and $x > 0.85$. Reitveld refinement analysis demonstrated that at intermediate doping levels a complex series of phases are present. The solubility limit of Sr in $CaAl_2O_4$ is rationalized in light of the structural studies. © 2002 Elsevier Science (USA)

INTRODUCTION

It can be argued that the importance of cement is only exceeded by our lack of knowledge as to the factors influencing the occurrence, structures and properties of the crystalline phases in common cements. With increasing pressure to use low-quality starting materials, e.g., fly ash and alternate fuels in the preparation of cements establishing the role of impurity cations in determining the key features of cement is becoming increasingly important (1). Whilst some volatile elements, e.g., Cd, Hg, Pb or Tl, will be lost during the formation of the clinker other less volatile elements, e.g., Sr, Ba are likely to become incorporated into the final product.

The complexity of cement means that the fate of such impurities often cannot be determined for commercially available materials. One approach that can be taken is to examine the effect dopant cations have on the properties of the individual phases and so develop a database that could eventually be applied to the analysis of commercial cements. In the present work, we have examined the crystal chemistry of the series $Ca_{1-x}Sr_xAl_2O_4$, that is we are concerned with the influence of Sr impurities in $CaAl_2O_4$. The $CaAl_2O_4$ is the main component of some high alumina cements, which are used in a wide range of applications in the construction and mining industries and especially in refractory castables for steel industry (2). The series $Ca_{1-x}Sr_xAl_2O_4$ is also of interest as hosts for long life phosphors (3).

[1]To whom correspondence should be addressed. Fax: 61-29351-3329. E-mail: b.kennedy@chem.usyd.edu.au.

EXPERIMENTAL

Synthesis

The series of 21 polycrystalline samples with the compositions $Ca_{1-x}Sr_xAl_2O_4$ ($x = 0$, 0.05, 0.1, 0.15, 0.2, 0.25, 0.3, 0.35, 0.4, 0.45, 0.5, 0.55, 0.6, 0.65, 0.7, 0.75, 0.85, 0.875, 0.9, 0.95 and 1) were prepared by solid state reaction of analytical grade $CaCO_3$ (Univar), $SrCO_3$ (Merck), and $Al(NO_3)_3 \cdot 9H_2O$ (Aldrich). For each composition, the appropriate stoichiometric quantities was very thoroughly mixed in an agate mortar for several minutes. The mixtures were then transferred to alumina crucibles and heated in air successively at 700°C, 800°C, 900°C and 1000°C, for 24 h each with regrinding after each heating step. Finally, the samples were heated in air at 1300°C for 72 h. $BaAl_2O_4$ was made in a similar manner.

X-Ray Powder Diffraction

All samples were characterized by X-ray powder diffraction using a Siemens D-5000 Diffractometer and Cu$K\alpha$ radiation. For selected examples additional high-resolution synchrotron powder X-ray diffraction data were collected using the Debye Scherrer camera at the Australian National Beamline Facility, Photon Factory, Japan (4). Samples were loaded into 0.5-mm glass capillaries that were rotated during the measurements. These measurements were performed under vacuum to minimize air scatter. This diffractometer is equipped with an automatic sample changer capable of holding eight samples. The BAS2000 Fuji image plates are 20 cm × 40 cm and each covers 40° in 2θ. A thin strip ~0.5 cm wide is used to record each diffraction pattern, and by translating the

0022-4596/02 $35.00

TABLE 1
Selected Structural Parameters for $Ca_{1-x}Sr_xAl_2O_4$ ($x = 0$ to 1), Obtained by Refinements Using Laboratory X-Ray Diffraction Data

$Ca_{1-x}Sr_xAl_2O_4$						Occupancy of Sr atoms (n^* observed)								
$x =$	Phase	a (Å)	b (Å)	c (Å)	β (°)	*M(1)*	*M(2)*	*M(3)*	% moles	R_p (%)	R_{wp} (%)	R_{exp} (%)	R_{Bragg} (%)	GOF
0	I	8.7083(6)	8.1000(5)	15.2065(9)	90.156(4)	0	0	0	100	13.01	17.70	12.95	3.95	1.87
0.05	I	8.7102(9)	8.1012(9)	15.216(2)	90.128(5)	0.01(8)	0	0.59(7)	100	12.28	16.44	12.12	3.93	1.84
0.1	I	8.725(1)	8.116(1)	15.218(2)	90.088(8)	0.07(9)	0	1.36(9)	100	11.62	15.56	11.73	3.13	1.78
0.15	I	8.730(1)	8.1226(9)	15.223(2)	90.077(8)	0.13(8)	0	1.72(7)	100	10.74	14.36	11.04	2.73	1.69
0.2	I	8.736(1)	8.132(2)	15.223(3)	90.066(8)	0.30(8)	0	2.30(7)	100	10.15	13.77	10.76	2.51	1.64
0.25	I	8.747(1)	8.147(1)	15.237(2)	90.04(1)	0.4(2)	0.1(1)	2.34(8)	100	9.97	13.19	10.42	2.41	1.60
0.3	I	8.751(1)	8.1589(9)	15.244(2)	90.05(1)	0.5(2)	0.3(2)	3.11(7)	100	9.69	13.15	10.20	2.48	1.66
0.35	I	8.760(1)	8.175(1)	15.251(2)	90.04(2)	0.6(2)	0.5(2)	3.1(1)	96(3)	9.20	12.48	10.04	2.51	1.54
	III	5.056(5)		8.352(6)		0.8(4)			4(1)				2.57	
0.4	I	8.768(1)	8.195(1)	15.277(2)	90.01(1)	0.9(1)	0.5(1)	3.2(1)	90(3)	8.96	12.00	9.64	2.09	1.55
	III	5.083(5)		8.360(5)		1.1(5)			10(1)				3.15	
0.45	I	8.770(1)	8.212(1)	15.296(2)	90.04(1)	0.9(1)	0.6(1)	3.7(1)	84(3)	9.73	12.76	9.44	2.78	1.83
	III	5.103(2)		8.359(1)		1.33(9)			16(1)				3.61	
0.5	I	8.815(1)	8.2168(9)	15.236(2)	89.632(5)	0.9(1)	1.0(1)	3.2(1)	79(2)	9.61	12.60	9.35	2.53	1.82
	III	5.103(1)		8.3609(9)		1.33(7)			21(1)				3.53	
0.55	I	8.8211(8)	8.2275(6)	15.245(1)	89.605(5)	0.9(1)	1.1(1)	3.2(1)	72(2)	9.91	13.36	9.20	3.32	2.11
	III	5.1030(7)		8.3686(5)		1.43(6)			28(1)				4.17	
0.6	I	8.8240(7)	8.2281(6)	15.250(1)	89.569(5)	0.9(1)	1.2(2)	3.3(2)	58(2)	9.76	12.67	9.23	3.42	1.89
	III	5.1032(5)		8.3736(8)		1.54(5)			42(2)				4.21	
0.65	I	8.8317(9)	8.2298(7)	15.259(2)	89.555(8)	0.9(1)	1.5(3)	3.5(2)	25(1)	9.36	12.47	9.04	3.52	1.90
	III	5.1061(4)		8.3806(3)		1.55(2)			30(1)				3.89	
	II	8.420(1)	8.818(2)	5.136(1)	93.58(1)	1.4(2)	1.48(2)		45(4)				4.18	
0.7	I	8.837(1)	8.233(1)	15.259(3)	89.44(1)	0.9(1)	1.5(4)	2.5(3)	9(1)	9.37	12.61	8.67	4.73	2.11
	III	5.1083(4)		8.3841(4)		1.58(2)			15(1)				3.96	
	II	8.4332(9)	8.834(1)	5.1401(9)	93.57(1)	1.4(2)	1.48(2)		76(4)				4.79	
0.75	III	5.1088(5)		8.4010(6)		1.59(7)			5(1)	7.93	10.58	8.74	2.04	1.46
	II	8.4140(5)	8.8129(5)	5.1442(3)	93.539(3)	1.62(6)	1.58(6)		95(2)				1.70	
0.85	III	5.1089(6)		8.4177(6)		1.60(8)			1.9(1)	7.74	10.30	8.77	1.52	1.38
	II	8.4061(5)	8.8064(5)	5.1451(3)	93.530(2)	1.67(6)	1.61(6)		98.1(3)				1.67	
0.875	II	8.4207(5)	8.8155(5)	5.1456(3)	93.518(2)	1.91(5)	1.78(5)		100	8.59	11.50	10.02	1.86	1.32
0.9	II	8.4202(6)	8.8164(6)	5.1479(3)	93.471(3)	1.94(6)	1.84(5)		100	8.83	11.35	8.59	2.38	1.75
0.95	II	8.4330(5)	8.8240(5)	5.1491(3)	93.411(3)	2	1.86(5)		100	8.51	11.00	8.40	2.20	1.71
1	II	8.4472(4)	8.8312(4)	5.1579(3)	93.395(2)	2	2		100	8.46	11.46	9.63	2.03	1.42

Note. I represents the phase isostructural with $CaAl_2O_4$, II, the phase isostructural with $SrAl_2O_4$, and III that isostructural with $BaAl_2O_4$. When fully occupied, $n = 4$ for those oxides isostructural with $CaAl_2O_4$ and $n = 2$ for the $SrAl_2O_4$and $BaAl_2O_4$-type phases.

image plate behind a Weissenberg screen, it is possible to collect around 20 diffraction patterns on each image plate. In this work we placed seven $Ca_{1-x}Sr_xAl_2O_4$ samples ($x = 0$, 0.125, 0.25, 0.5, 0.75, 0.875 and 1) together with a Si standard in the sample changer and collected data at a wavelength of 0.9987 Å.

Neutron Powder Diffraction

Neutron diffraction data were collected for three samples $x = 0$, 0.5 and 0.85 using the HB-4 high-resolution powder diffractometer at the Oak Ridge National Laboratory. For each of the compounds studied, about 10 g of powder were contained in a thin-walled, 13 mm diameter, vanadium sample can. Diffraction patterns were recorded, using neutrons of wavelength 1.505 Å, over the 2θ range from 11° to 135°, with a step size of 0.05°.

Structural Refinements

The structural refinements were performed using the Rietveld method with the PC version of the program Rietica (5). The background was defined by a fourth-order polynomial in 2θ and was refined simultaneously with the profile parameters. A pseudo-Voigt function was chosen to generate the profiles. The Gaussian component has widths given by the function $(\text{FWHM})^2 = U\tan^2\theta + V\tan\theta + W$ where U, V and W are refineable parameters. The results of the Rietveld refinements using the laboratory X-ray diffraction data are summarized in Table 1.

RESULTS AND DISCUSSION

Initial attempts to refine structures of the compounds $Ca_{1-x}Sr_xAl_2O_4$ by the Rietveld method using conventional laboratory X-ray measurements met with mixed success.

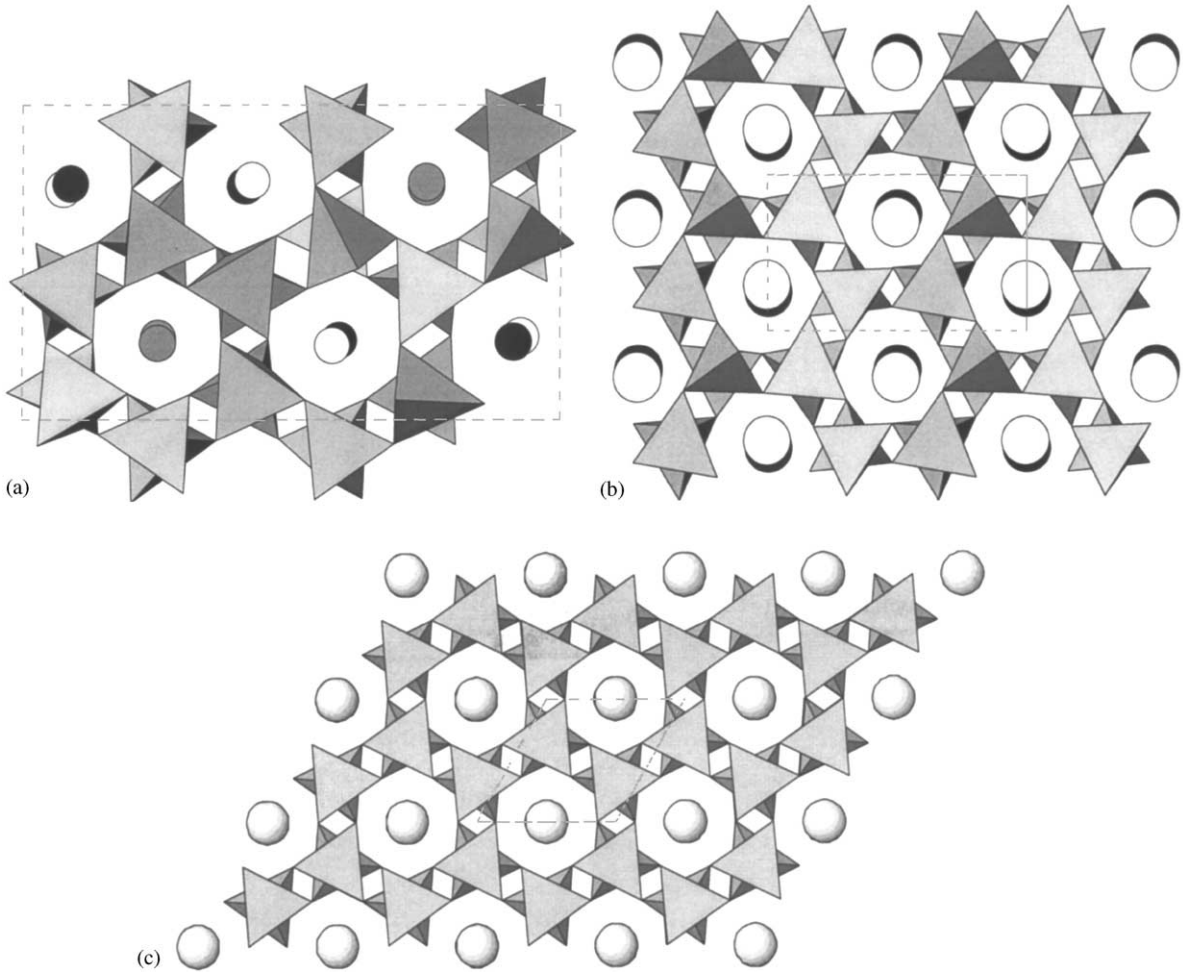

FIG. 1. (a) Projection along [010] for $CaAl_2O_4$. The open circles represent $M(1)$, the solid circles, $M(2)$, and the shaded circles, $M(3)$. (b) Projection along [010] for $SrAl_2O_4$. Both the $M(1)$ and $M(2)$ atoms are located within the one channel. (c) Projection along [001] for $BaAl_2O_4$. The single $M(1)$ type atoms are indicated by the circles.

Consequently higher resolution synchrotron diffraction patterns were collected for a number of samples. These synchrotron powder X-ray diffraction patterns revealed a complex series of oxides to be present. Once the phases present had been identified from the synchrotron diffraction studies, it was possible to develop suitable models for the analysis of the laboratory X-ray diffraction data, Table 1. This enabled the phase diagram in the series $Ca_{1-x}Sr_xAl_2O_4$ to be established.

Three phases were found to be present in the solid solutions and these were isostructural with $CaAl_2O_4$, $SrAl_2O_4$ and $BaAl_2O_4$. Despite the fact that both Ca and Sr are smaller than Ba at critical compositions, the phases formed were isostructural with the pure Ba oxide phase. The three structures $CaAl_2O_4$, $SrAl_2O_4$ and $BaAl_2O_4$ all contain a similar motif consisting of rings formed by six corner-sharing AlO_4 tetrahedra, Fig. 1. The structures differ in the arrangement of the divalent cations within the channels formed by the AlO_4 rings. $CaAl_2O_4$ has a monoclinic structure in space group $P21/n$ with $a = 8.7001(4)$, $b = 8.0943(4)$, $c = 15.2074(8)$ Å, and $\beta = 90.156(2)^\circ$. These values compare favorably with those reported previously (6). In this structure there are three distinct cation sites, Fig. 1a. Two of these, labeled $M(1)$ and $M(2)$, are six-coordinate, the O anions coming from four different AlO_4 tetrahedra. These are ordered within one of the channels formed by the AlO_4 rings. The third cation, $M(3)$ is located within the second channels (Fig. 1a) and is surrounded by nine oxygen atoms from five different AlO_4 tetrahedra. Of the nine oxygen atoms six are shared by two $M(3)$ cations forming an elongated octahedron, thereby forming a continuous chain of the type $M(3)$–O–$M(3)$. The remaining three oxygen atoms lie in a plane at right angles to the chain.

At low Sr doping levels, $x < 0.35$, the diffraction patterns demonstrate that the only products formed are the solid solutions of the type $Ca_{1-x}Sr_xAl_2O_4$, Fig. 2. Rietveld structural refinements of X-ray diffraction data are ideally suited to identify and quantify the site occupancies of Ca and Sr as a result of the relative large difference in the atomic numbers, and hence X-ray scattering factors, of Ca and Sr. Where such disorder was observed the atoms were constrained to occupy identical positions and to have identical displacement parameters. The Rietveld refinements, Fig. 3, of these structures demonstrated that the larger Sr cations predominately occupied the higher coordination $M(3)$ sites. A similar effect is noticed when Sr replaces Ca in $Ca_3Al_2O_6$ (7). The present structural refinements show that this substitution is accompanied by a small decrease in the average $M(1)$ and $M(2)$–O distances and a concurrent small increase in the average $M(3)$–O distance as the Sr content increases. Although individual bond lengths are obtained from the refinements using the

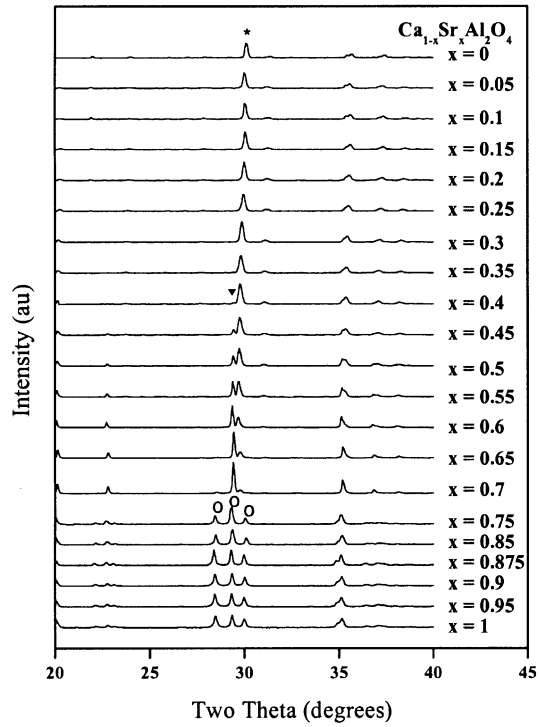

FIG. 2. Laboratory powder X-ray diffraction patterns for $Ca_{1-x}Sr_xAl_2O_4$. The *, ▼ and ○ show the strongest peaks for the $CaAl_2O_4$, $SrAl_2O_4$ and $BaAl_2O_4$-type structures, respectively. The patterns were collected using Cu$K\alpha$ radiation (1.54 Å).

laboratory X-ray diffraction data these, not unexpectedly, show some scatter and a discussion of the variation in these is not warranted. The higher resolution synchrotron data provided more reliable results for the small number of samples studied this way. In $CaAl_2O_4$, each of the 21 crystallographically unique atoms occupies a general xyz position. Consequently, the structural refinements involved over 100 refineable parameters including 63 positional parameters and 21 atomic displacement parameters. This large number of variables limits the precision with which the individual M–O bond distances can be deduced from the powder X-ray diffraction data. In order to verify the validity of the structural model used for $CaAl_2O_4$, we also examined this material using powder neutron diffraction data. This provided a more precise estimate of the positional parameters, especially for the lighter oxygen atoms. The positional parameters from the two refinements were in reasonable agreement with each other, based on the esds of the refined parameters.

In the $x = 0.35$ sample, a very weak feature is observed near $2\theta = 21^\circ$ suggesting a second phase may be present. This feature is clearly evident in the $x = 0.4$ sample, Fig. 2. Since the three M cations all occupy general positions within the cell there is an equal number of each of these. As a consequence of the strong preference of the Sr cations for the $M(3)$ sites at $x = 0.33$, the $M(3)$ position will be filled

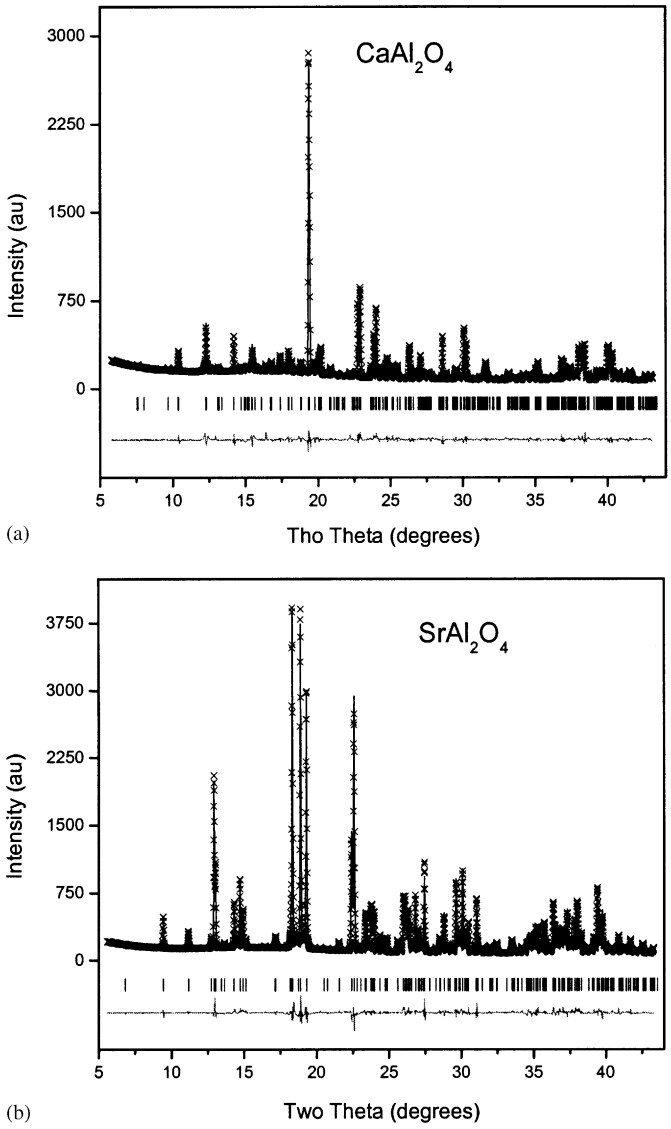

FIG. 3. Observed (crosses) calculated and difference (solid lines) synchrotron diffraction profiles for $CaAl_2O_4$ (R_p 6.48, R_{wp} 8.60%) and $SrAl_2O_4$ (R_p 5.36, R_{wp} 5.88%). The vertical markers show the positions of all the allowed Bragg reflections. Since the patterns were collected at 0.9987 Å the peaks seen in Fig. 2 or 4 near 30° are near 19°.

with Sr and it appears that the Sr cations are too large to occupy the other channel in which the $M(1)$ and $M(2)$ cations lie, Fig. 4. We believe that the inability for Sr to occupy these lower coordination sites is a significant factor in limiting the solubility of Sr in $CaAl_2O_4$.

The refinements from the X-ray data did provide precise lattice parameters. A smooth increase in the a, b and c parameters was observed as the Sr content increased towards 0.33 whilst the monoclinic angle, β, decreased towards 90°, Fig. 5. These trends continued past $x = 0.35$, i.e., after the $M(3)$ site was fully occupied, up to $x = 0.5$, demonstrating some Sr does occupy the $M(1)$ and $M(2)$ sites, although the refinements were inconclusive in this regard. Figure 5 illustrates a clear discontinuity in the refined lattice parameters for this phase in the samples above $x = 0.5$.

Examination of the difference profiles obtained by Rietveld analysis of the synchrotron diffraction data for $Ca_{0.6}Sr_{0.4}Al_2O_4$ assuming only a $P21/n$-type phase was present suggested that the additional phase was hexagonal. The intensities of the peaks due to this hexagonal phase, seen in the difference profiles, was observed to progressively increase as the Sr content was increased, and it was concluded that the samples with Sr contents $0.35 \leq x \leq 0.65$ were two phase mixtures. $SrAl_2O_4$ has a polymorph with a hexagonal structure although this is only observed at temperatures above 700°C (8). This hexagonal structure is also observed in $BaAl_2O_4$ at room temperature (9). Analysis of the diffraction data using such a two-phase model yielded satisfactory fits, Fig. 6. Again the validity of this model was verified for the $x = 0.5$ sample using powder neutron diffraction methods.

There is only one cation site within the channels of the hexagonal structure (Fig. 1c). Whilst it was not possible to unequivocally determine the Ca:Sr ratio within these channels, the final fits assumed that 33% of the Sr was present in the monoclinic $P21/n$ phase and the remainder was in the hexagonal phase. The refined lattice parameters for the hexagonal phase, space group $P6_322$, in the $x = 0.5$ sample were $a = 5.097(1)$ $c = 8.358(2)$ Å. These values are noticeably smaller than

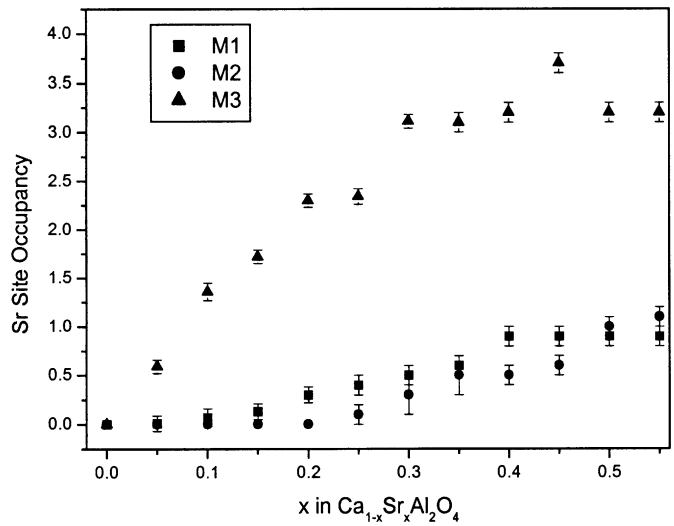

FIG. 4. Variation in the refined cation site occupancies for the $CaAl_2O_4$-type phase in the series $Ca_{1-x}Sr_xAl_2O_4$ obtained from the Rietveld analysis. Below $x \approx 0.3$ neither the $M(1)$ nor $M(2)$ site is appreciably occupied by Sr, with all the Sr occupying the larger $M(3)$ site. At higher Sr levels, the occupancy of the $M(3)$ site is effectively constant.

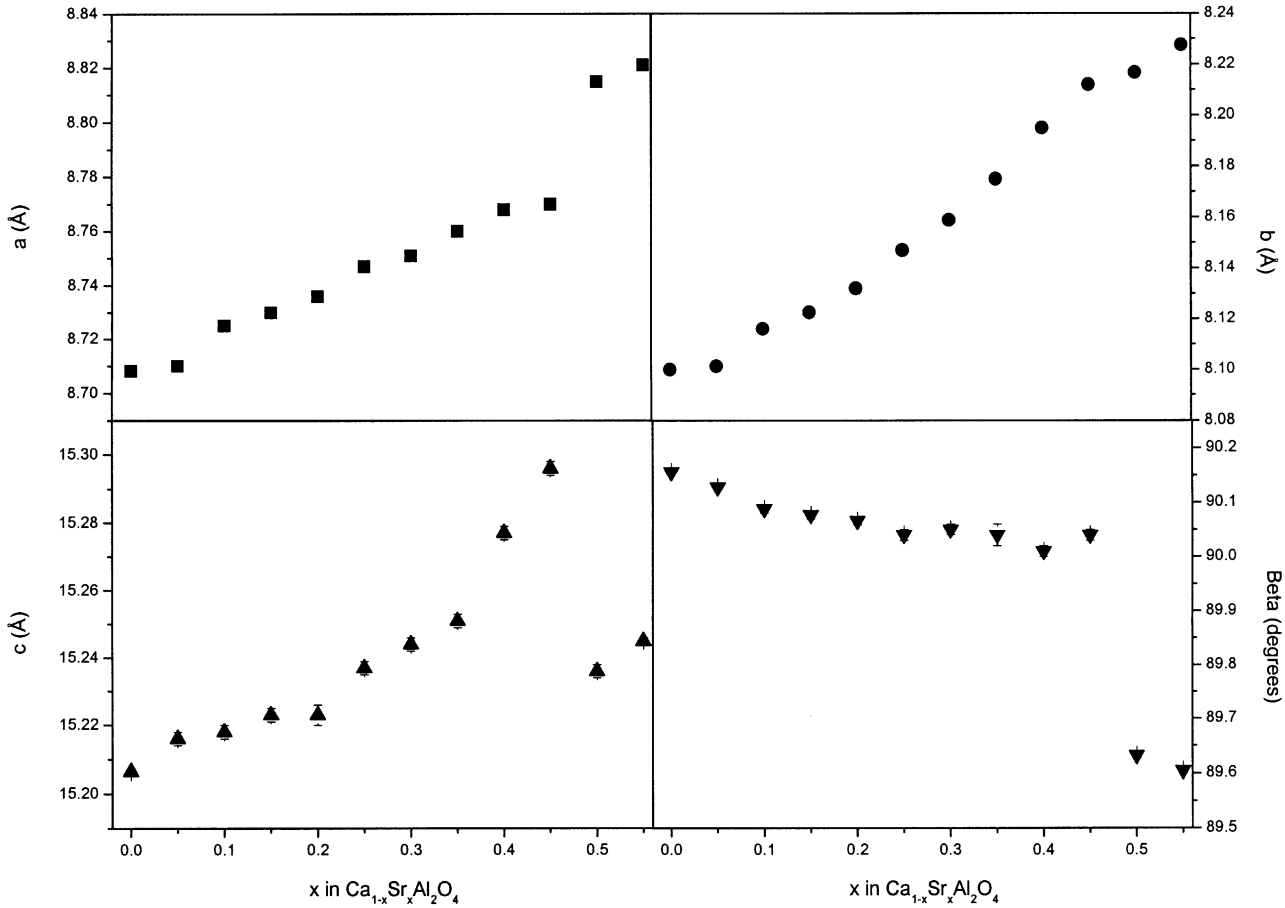

FIG. 5. Variation in the lattice parameters for the $CaAl_2O_4$-type phase in the series $Ca_{1-x}Sr_xAl_2O_4$ as the Sr content is increased. The discontinuity near $x \approx 0.5$ reflects the upper limit of stability for this phase.

those reported for pure $BaAl_2O_4$ (9), $a = 5.2252$, $c = 8.7925$ Å. This is not surprising since both Ca and Sr are considerably smaller than Ba. Likewise the size of the monoclinic $P21/n$ phase in the $x = 0.5$ sample is larger, $a = 8.771(1)$, $b = 8.210(1)$, $c = 15.310(2)$ Å, $\beta = 90.02(1)^\circ$, than that observed in pure $CaAl_2O_4$ due to the larger size of Sr relative to Ca.

As the Sr content increases beyond $x = 0.35$, the amount of the monoclinic $P21/n$ phase present decreased rapidly with a concurrent increase in the amount of the hexagonal phase present, Fig. 7. In the $x = 0.6$ sample, c.a. 40% of the sample was hexagonal. Attempts to fit the diffraction pattern for the $x = 0.65$ sample with the two phase (hexagonal + monoclinic $P21/n$) model were unsuccessful. Considering the Sr-rich compounds, then the diffraction patterns for the four samples with $x \geq 0.875$ were well fitted with the monoclinic $P2_1$ $SrAl_2O_4$ model (10), Fig. 3. Whilst there are two cation sites within the channels formed by the rings of AlO_4 tetrahedra in the $SrAl_2O_4$ structure these sites are very similar. Both cation sites have nine neighboring O atoms coming from six-different AlO_4 tetrahedra. The $M(1)$–O and $M(2)$–O bond distances both vary over a wide range 2.45–3.56 Å for $M(1)$–O and 2.52–3.6 Å for $M(2)$–O. In general, the average $M(1)$–O bond distances are ~0.1 Å longer than that of $M(2)$–O. Nevertheless, there is no noticeable preference of the Ca or Sr for either site. Consequently, the final analysis assumed a statistical distribution of Ca and Sr over the two sites. Again the large number of variable parameters limited the precision with which the M–O bond distances could be estimated.

In the $x = 0.85$ sample, three peaks are observed near $2\theta = 28.5^\circ$, 29.4° and 30.1° in an apparent ratio of 3:5:2, Fig. 6. It was not possible to fit this ratio using a single-phase model. To fit this region, as well as rest of the diffraction pattern, it was necessary to consider that the peak near $2\theta = 29.4^\circ$ is a combination of the 121 and 220 Bragg reflections from a hexagonal, $BaAl_2O_4$-type structure and the 012 reflection from a monoclinic $SrAl_2O_4$-type phase. The reflection at $2\theta = 29.4^\circ$ is noticeably wider that that at $2\theta = 30.1^\circ$, demonstrating the overlap of a number

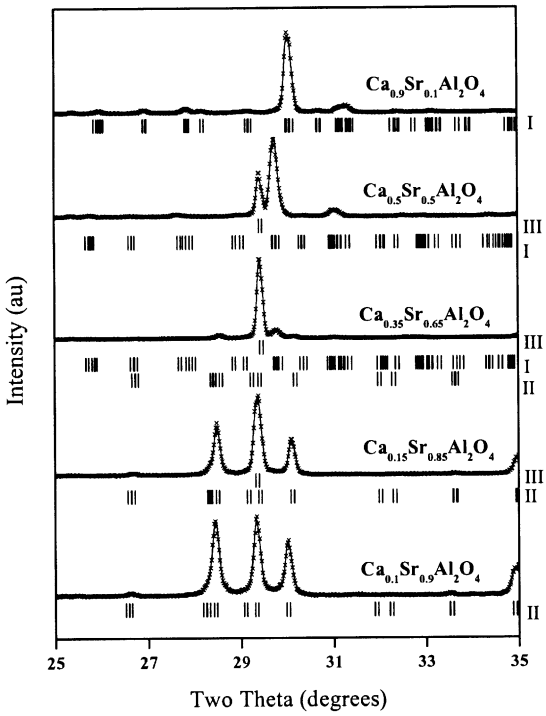

FIG. 6. Part of the observed laboratory powder X-ray diffraction and calculated profiles for selected examples. This figure highlights the differences between the three phases: the Bragg reflections for the appropriate phases are shown below each profile. The Roman numerals to the right of the patterns indicate which phase is responsible for which Bragg reflections. I shows the reflection markers due to the $CaAl_2O_4$-type phase, II those from the $SrAl_2O_4$-type phase and III from the $BaAl_2O_4$-type phase. The patterns were collected using Cu$K\alpha$ radiation (1.54 Å).

of reflections. A powder neutron diffraction pattern was also collected for this sample. The refinements from this yielded the following lattice parameters: for the hexagonal phase $a = 5.1011(9)$, $c = 8.378(2)$ Å and for the monoclinic $P2_1$ phase $a = 8.394(1)$, $b = 8.793(1)$, $c = 5.1356(8)$ Å, $\beta = 93.606(7)^\circ$. We observe a small increase in the size of the hexagonal cell relative to that seen in the $x = 0.5$ sample, whilst the monoclinic cell is noticeably smaller than that found for pure $SrAl_2O_4$, $a = 8.4402(3)$, $b = 8.8204(3)$, $c = 5.1557(2)$ Å, $B = 93.410(1)^\circ$ in keeping with the size differences between Sr and Ca.

This two-phase (hexagonal and monoclinic $P2_1$) model also proved satisfactory in the fitting of the diffraction pattern for the $x = 0.75$ sample, but did not yield satisfactory fits to the patterns for the $x = 0.70$ or 0.65 samples. The diffraction patterns for these two samples could only be adequately modeled using a three phase mixture (hexagonal and the two monoclinic phases $P21/n$ and $P2_1$). The final phase-composition relationship is illustrated in Fig. 7.

In conclusion, we have demonstrated there is a complex series of phases formed when Sr is added to $CaAl_2O_4$. The present results for the Ca-rich oxides are in general, but not perfect agreement, with the conclusions of Ju and co-workers (11). We have observed the Sr preferentially occupies a single site in the $CaAl_2O_4$ structure, while this site is unfilled single-phase samples are obtained. Once this site fills, near $x = 0.33$ in $Ca_{1-x}Sr_xAl_2O_4$, a second phase hexagonal phase is also present. This limit is lower than that described by Ju et al. (11), who concluded that a single phase exists up to $x = 0.5$. Their published X-ray diffraction patterns are very similar to those found in the present work and scrutiny of their Fig. 1 shows the presence of a second phase in the $x = 0.5$ sample contrary to their stated conclusion (11). In the present work only at very high Sr levels are single-phase samples of $SrAl_2O_4$ obtained. Further studies of the relative stability of the

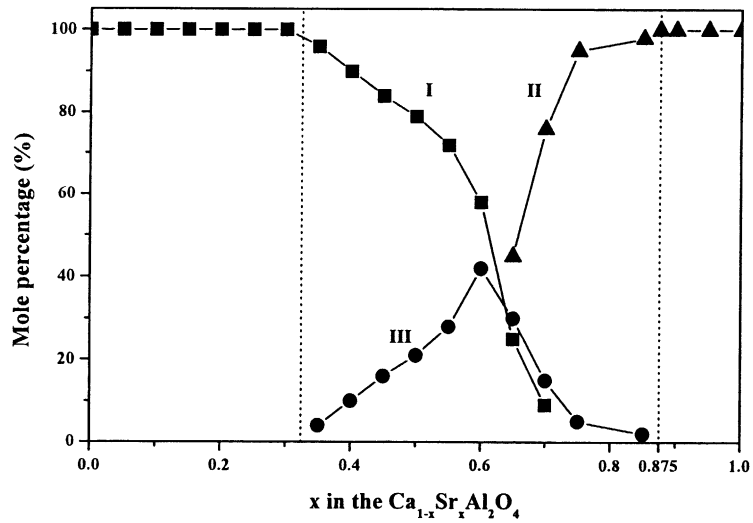

FIG. 7. Mole percentage versus x in the $Ca_{2-x}Sr_xAl_2O_4$. **I** represents phases isostructural with $CaAl_2O_4$, **II** $SrAl_2O_4$, and **III** $BaAl_2O_4$.

three phases, especially at elevated temperatures would be interesting.

ACKNOWLEDGMENTS

We thank Bryan Chakoumakos (ORNL) for recording the powder neutron diffraction data. The synchrotron measurements at the Australian National Beamline Facility were supported by the Australian Synchrotron Research Program which is funded by the commonwealth of Australia under the Major National Research Facilities Program. Oak Ridge National Laboratory is managed by UT-Battelle, LLC, for the US Department of Energy under Contract No. DE-AC05-00OR22725.

REFERENCES

1. N. Bouzoubaa, M. H. Zhang, A. Bilodeau, and V. M. Malhotra, *Cem. Concr. Res.* **28,** 1555 (1998).
2. B. M. Mohamed and J. H. Sharp, *J. Mater. Chem.* **7,** 1595 (1997).
3. J. Holsa, H. Jungner, M. Latusaari, and J. Niittykoski, *J. Alloys Compd.* **323–324,** 326 (2001).
4. T. M. Sabine, B. J. Kennedy, R. F. Garrett, G. J. Foran, and D. J. Cookson, *J. Appl. Crystallogr.* **28,** 513 (1995).
5. B. A. Hunter and C. J. Howard, "A Computer Program for the Rietveld Analysis of X-ray and Neutron Powder Diffraction Patterns." 1996.
6. W. Horkner and H. K. Muller-Buschbaum, *J. Inorg. Nucl. Chem.* **38,** 983 (1976).
7. A. K. Prodjosantoso, B. J. Kennedy, and B. A. Hunter, *Aust. J. Chem.* **53,** 195 (2000).
8. S. Ito, S. Banno, K. Suzuki, and M. Inagaki, *Z. Physik. Chem. Neu. Folg.* **105,** 173 (1977).
9. A. J. Perrota and J. V. Smith, *Bull. Soc. Mineral. Cristallogr.* **91,** 85 (1968).
10. V. A. R. Schulze and H. Muller-Buschbaum, *Z. Anorg. Allg. Chem.* **475,** 205 (1981).
11. S. H. Ju, J. C. Kim, J. C. Choi, H. L. Park, S. I. Mho, and T. W. Kim, *Mater. Res. Bull.* **34,** 1905 (1999).